Fluorescence Lifetime Measurements and Spectral Analysis of Adamantyldiazirine

Jeffrey S. Buterbaugh,[†] John P. Toscano,[†,§] William L. Weaver,[‡] James R. Gord,[‡] Christopher M. Hadad,*[,†] Terry L. Gustafson,*[,†] and Matthew S. Platz*[,†]

Contribution from the Department of Chemistry, The Ohio State University, 100 West 18th Avenue, Columbus, Ohio 43210-1185, and Wright Laboratories, Building 490, 1790 Loop Road North, Wright-Patterson AFB, Ohio 45433-7103

Received November 20, 1996[⊗]

Abstract: We report the first confirmed fluorescence lifetime measurement for a diazirine. We have obtained time-correlated single-photon counting fluorescence decays for adamantyldiazirine in a variety of solvents, over a wide range of temperatures (77−320 K) and across the diazirine absorption band (330−371 nm). The fluorescence lifetime of the primary decay component is on the order of 240 ps at ambient temperature and increases at lower temperatures. Arrhenius treatment of the fluorescence lifetime data indicates that the rate-limiting barrier for activated processes in the diazirine excited state is between 2.7 and 2.9 kcal/mol. Adamantyldiazirine's fluorescence lifetime appears to be unaffected by deuteration of the solvent, solvent polarity, or excitation energy. We also report and discuss the steady-state absorption and fluorescence emission spectra of adamantyldiazirine in a variety of solvents, as well as the infrared spectrum (KBr). We interpret the spectra with the help of *ab initio* (RHF/6-31G* and CIS/6-31G*), density functional (B3LYP/6-31G*), and semiempirical (PM3) calculations. The fluorescence quantum yield of adamantyldiazirine at ambient temperature was calculated to be ∼0.0012. Analysis of our data in the light of previous research leads us to conclude that little or no *inter*molecular chemistry is attributable to photoexcited adamantyldiazirine in solution at ambient temperature. Rather, fluorescence competes with one or more *intra*molecular photochemical processes.

Introduction

The chemistry of carbene intermediates has been of considerable interest to organic chemists since their involvement in the alkaline hydrolysis of chloroform was demonstrated by Hine *et al*. in the middle of this century.[1] These highly-reactive species are now widely used in synthesis and may be generated by photolyzing an appropriate diazirine. Molecular nitrogen is released upon photoexcitation, and a transient carbene is created. However, it is often difficult to distinguish between the chemistry of the carbene and the excited state of its diazirine precursor.[2,3] Indeed, there are several possible decay pathways from the excited state of a diazirine. Some of these processes are illustrated in Scheme 1. These include, but are not necessarily limited to, fluorescence, internal conversion, intersystem crossing, carbon−nitrogen bond scission[4] followed by *intra*molecular rearrangement processes (*e.g.*, to form a diazo compound or, coupled with nitrogen loss, alkene formation *via* 1,2-hydrogen migration), *inter*molecular reactions (*e.g.*, with solvent or other diazirines), and simple nitrogen extrusion to generate the carbene intermediate. The picture is further complicated by the fact that many of the possible products of these reactions are also accessible *via* the carbene. These complexities have made a comprehensive understanding of diazirine photochemistry an elusive goal.

Scheme 1

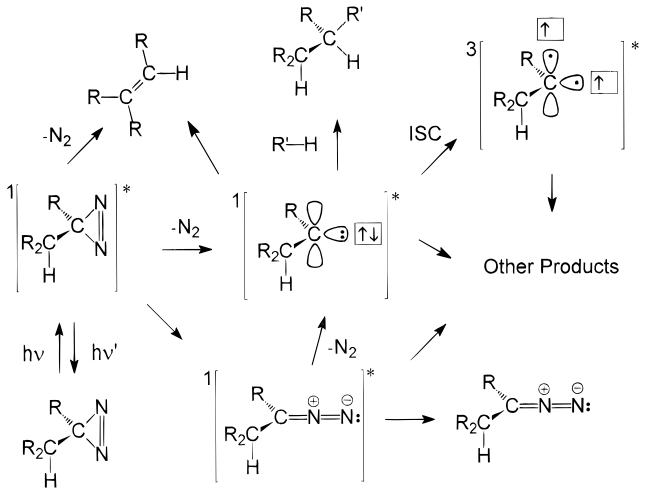

Diazirines are weakly absorbing chromophores, and often exhibit weak fluorescence.[5−10] The fluorescence lifetime of a diazirine should therefore serve as an indirect probe of other excited-state processes. Any enhancement of a competing process should be manifested as a decrease in the diazirine fluorescence lifetime, and any retardation of an alternate decay pathway should result in an increase in the lifetime.

[†] The Ohio State University.

[§] Current address: Department of Chemistry, Johns Hopkins University, 3400 North Charles Street, Baltimore, MD 21218-2685.

[‡] Wright-Patterson AFB.

[⊗] Abstract published in *Advance ACS Abstracts,* April 1, 1997.

(1) Hine, J. *Divalent Carbon*; Ronald Press: New York, NY, 1964; pp 1−206.

(2) Frey, H. M. *Adv. Photochem.* **1966**, *4*, 225−256.

(3) Morgan, S. C.; Jackson, J. E.; Platz, M. S. *J. Am. Chem. Soc.* **1991**, *113*, 2782−2783.

(4) Yamamoto, N.; Bernardi, F.; Bottoni, A.; Olivucci, M.; Robb, M. A.; Wilsey, S. *J. Am. Chem. Soc.* **1994**, *116*, 2064−2074.

(5) Modarelli, D. A.; Morgan, S. C.; Platz, M. S. *J. Am. Chem. Soc.* **1992**, *114*, 7034−7041.

(6) Figuera, J. M.; Perez, J. M.; Tobar, A. *J. Chem. Soc., Faraday Trans. 1* **1978**, *74*, 809−817.

(7) Hepburn, P. H.; Hollas, J. M.; Thakur, S. N. *J. Mol. Spectrosc.* **1975**, *54*, 483−492.

(8) Mirbach, M. J.; Liu, K.-C.; Mirbach, M. F.; Cherry, W. R.; Turro, N. J.; Engel, P. S. *J. Am. Chem. Soc.* **1978**, *100*, 5122−5129.

(9) Sieber, H.; Moomaw, W. R.; Neusser, H. J.; Schlag, E. W. *J. Phys. Chem.* **1991**, *95*, 6958−6961.

(10) Merritt, J. A. *Can. J. Phys.* **1962**, *40*, 1683−1684.

S0002-7863(96)04022-X CCC: $14.00

Adamantyldiazirine has attracted the attention of several investigators.[3,11−16] This is due, in part, to the fact that adamantyldiazirine is easy to synthesize, and is a stable, crystalline solid that is easy to handle. The carbene anticipated from the fragmentation of the diazirine must surmount substantial barriers to intramolecular rearrangement of carbon or hydrogen, owing to the highly strained nature of the products of such reactions. As a result, the carbene is expected to have a long lifetime and useful intermolecular chemistry.[17] Bayley and Knowles have used adamantyldiazirine in membrane-labeling studies[11,12] and Brinker *et al*. have analyzed the photolysis products in the cavities of β-cyclodextrins and various zeolites.[14,15] Recently, Bonneau and Liu have made an important contribution to the understanding of adamantyldiazirine's photochemistry.[16] They have measured the quantum yields of formation for the transient species 2-diazoadamantane ($\phi_{\text{diazo}} \sim 0.5$) and adamantylidene ($\phi_{\text{carbene}} \sim 0.5$) in isooctane solutions. Previous studies had only analyzed the stable photoproducts.[13−15,18] These stable photoproducts vary with solvent. Some of the most commonly observed are adamantanone, adamantanone azine, 2,4-dehydroadamantane, and solvent insertion products. We have focused our interest primarily on the structure, kinetics, and chemistry of the photoexcited diazirine and subsequently generated transient species.[3] Adamantyldiazirine, as per adamantylidene, will resist hydrogen and carbon migrations due to its rigid architecture. For this reason, it is an attractive candidate for spectroscopic analysis.

The time-correlated single-photon counting (TCSPC) method is capable of measuring fluorescence lifetimes in the picosecond regime, and its excellent signal-to-noise ratio makes it useful even for weak fluorophores. Consequently, it is an ideal probe to interrogate the excited state of adamantyldiazirine.

Experimental and Computational Methods

All of the solvents employed were obtained from Burdick and Jackson or Aldrich (Freon-113 and methylcyclohexane) and were used without further purification. None of the solvents exhibited significant fluorescence, and interference from solvent Raman bands was avoided in the measurement of fluorescence lifetimes by careful selection of the excitation and monitoring wavelengths. Adamantyldiazirine was prepared according to literature processes.[11,12,19]

Absorption spectra were collected on either a Milton-Roy Spectronic-3000 array spectrophotometer (accuracy $\leq$0.35 nm; precision $\pm$0.0005 nm) or (in a few cases) a Hewlett-Packard HP8452A diode array spectrophotometer (accuracy 2.0 nm; precision 0.05 nm). Steady-state fluorescence excitation and emission spectra were measured on a SPEX Fluorolog-2. The excitation source was a 450-W xenon lamp (SPEX 1907-OFR), passed through a single-grating monochromator (SPEX 1681B Minimate; 1200 groove/mm; 3.77 nm/mm). Fluorescence was detected in a T-box sampling module (SPEX 1692T) at 90° relative to the excitation through a double-grating monochromator (SPEX 1680B Spectramate; 1200 groove/mm; 1.70 nm/mm) with a SPEX 1911F detector. The slit widths were invariably 1.25 mm, so the excitation band-pass was 4.7 nm and the emission band-pass was 2.1 nm. Rough quantum yield calculations were performed according to standard methods.[20] No corrections were made for the average detector response or for the wavelength dependence of the solvent refractive indices. The fluorescence yield ($\phi_F = 0.44$) of diphenylbutadiene (DPB) in cyclohexane was used as a standard.[21]

The infrared spectrum was measured in a 275-mg KBr pellet (10 mg of adamantyldiazirine) with a Bruker Equinox-55 infrared microscope, model No. A590, operating in reflection mode. The spectrum was obtained from 512 scans with the instrument set at 0.5-cm^{-1} resolution, although the specifications of the instrument only guaranteed 4-cm^{-1} resolution in reflection mode.

Ab initio and density functional calculations[22−25] were performed using *Gaussian 94*,[26] while semiempirical calculations were run either with *Gaussian 94* or with *HyperChem*, release 4.5. In *HyperChem*, the PM3 method was used in Restricted Hartree−Fock calculations. Configuration interaction was included for eight occupied and eight unoccupied orbitals. The ground-state optimized geometry was used in the calculation of S_0, S_1*, and T_1*. The gradient of the reference configuration was <0.009 kcal/mol/Å.

In *Gaussian 94*, the frozen-core (fc) approximation was used for all correlated geometries and the basis set employed was the standard 6-31G*. Excited state calculations utilized the Configuration Interaction with Single Excitations (CIS) method within the frozen-core approximation.[27−31]

All fluorescence lifetimes were determined using a time-correlated single-photon counting (TCSPC) instrument (Figure 1). For experiments conducted at The Ohio State University, the pulse train of a synchronously-pumped cavity-dumped dye laser (Coherent 700 Series; Rhodamine 6-G or DCM) was directed to a beam splitter. A portion of the pulse train was routed to a fast photodiode that registered a "start" signal on a Time-to-Amplitude Converter (TAC; Tennelec TC-864) after passing through a Constant Fraction Discriminator (CFD; Tennelec TC-455). This established the time position of each pulse with great precision. The "start" pulses initiated the charging of a capacitor in the TAC. The remainder of the pulse train was frequency doubled in an appropriate nonlinear crystal (Inrad, RDA) to generate UV excitation within the diazirine absorbance band. Fluorescence was detected at 90° after having passed through a polarization analyzer (oriented at 54.7° relative to the polarization of the laser excitation), a depolarizer, and a subtractive double monochromator (American Holographic DB-10S). The detector was a Microchannel Plate Photomultiplier Tube (MCP-PMT; Hammamatsu R-2809U-07). The signals arising from single photons were amplified (Minicircuit ZHL-42) and passed through a second CFD. The CFD output pulses then served as the "stop" signals for the capacitor in the TAC. The TAC capacitance was transferred to a Multi-Channel Analyzer (MCA; Tennelec PCA-II), where the data were binned and presented as a histogram. This histogram served as a representation of the fluorescence decay.

(11) Bayley, H. B.; Knowles, J. R. *Biochemistry* **1980**, *19*, 3883−3892.
(12) Bayley, H. B.; Knowles, J. R. *Biochemistry* **1978**, *17*, 2420−2423.
(13) Isaev, S. D.; Sherstyuk, V. P.; Koslov, O. F.; Skripkin, V. V.; Yanku, I. *Teor. Eksp. Khim.* **1991**, *27*, 211−220.
(14) Brinker, U. H.; Kolodziejczyk, M.; Poliks, M. D. *Angew. Chem., Int. Ed. Engl.* **1993**, *32*, 1344−1345.
(15) Kupfer, R.; Poliks, M. D.; Brinker, U. H. *J. Am. Chem. Soc.* **1994**, *116*, 7393−7398.
(16) Liu, M. T. H.; Bonneau, R. *J. Am. Chem. Soc.* **1996**, *118*, 7229−7230.
(17) Moss, R. A.; Chang, M. J. *Tetrahedron Lett.* **1981**, *22*, 3749−3752.
(18) Morgan, S. C. Dissertation, 1992, The Ohio State University, pp 1−256.
(19) Isaev, S. D.; Yurchenko, A. G.; Stepanov, F. N.; Kolyada, G. G.; Novikov, S. S.; Karpenko, N. F. *J. Org. Chem. USSR* **1973**, *9*, 745−748.
(20) Karpovich, D. S.; Blanchard, G. J. *J. Phys. Chem.* **1995**, *99*, 3951−3958.
(21) Birks, J. B.; Dyson, D. J. *Proc. R. Soc. (London) A* **1963**, *275*, 135−148.
(22) Stephens, P. J.; Devlin, F. J.; Chabalowski, C. F.; Frisch, M. J. *J. Phys. Chem.* **1994**, *98*, 11623−11627.
(23) Becke, A. D. *J. Chem. Phys.* **1993**, *98*, 5648−5652.
(24) Lee, C.; Yang, W.; Parr, R. G. *Phys. Rev. B* **1988**, *37*, 785−789.
(25) Ziegler, T. *Chem. Rev.* **1991**, *91*, 651−667.
(26) *Gaussian 94*, Revision D.3; Frisch, M. J.; Trucks, G. W.; Schlegel, H. B.; Gill, P. M. W.; Johnson, B. G.; Robb, M. A.; Cheeseman, J. R.; Keith, T.; Petersson, G. A.; Montgomery, J. A.; Raghavachari, K.; Al-Laham, M. A.; Zakrzewski, V. G.; Ortiz, J. V.; Foresman, J. B.; Cioslowski, J.; Stefanov, B. B.; Nanayakkara, A.; Challacombe, M.; Peng, C. Y.; Ayala, P. Y.; Chen, W.; Wong, M. W.; Andres, J. L.; Replogle, E. S.; Gomperts, R.; Martin, R. L.; Fox, D. J.; Binkley, J. S.; Defrees, D. J.; Baker, J.; Stewart, J. P.; Head-Gordon, M.; Gonzalez, C.; Pople, J. A. 1995.
(27) Foresman, J. B.; Head-Gordon, M.; Pople, J. A.; Frisch, M. J. *J. Phys. Chem.* **1992**, *96*, 135−149.
(28) Hadad, C. M.; Foresman, J. B.; Wiberg, K. B. *J. Phys. Chem.* **1993**, *97*, 4293−4312.
(29) Wiberg, K. B.; Hadad, C. M.; Ellison, G. B.; Foresman, J. B. *J. Phys. Chem.* **1993**, *97*, 13586−13597.
(30) Walters, V. A.; Hadad, C. M.; Thiel, Y.; Colson, S. D.; Wiberg, K. B.; Johnson, P. M.; Foresman, J. B. *J. Am. Chem. Soc.* **1991**, *113*, 4782−4791.
(31) Wiberg, K. B.; Hadad, C. M.; Foresman, J. B.; Chupka, W. A. *J. Phys. Chem.* **1992**, *96*, 10756−10768.

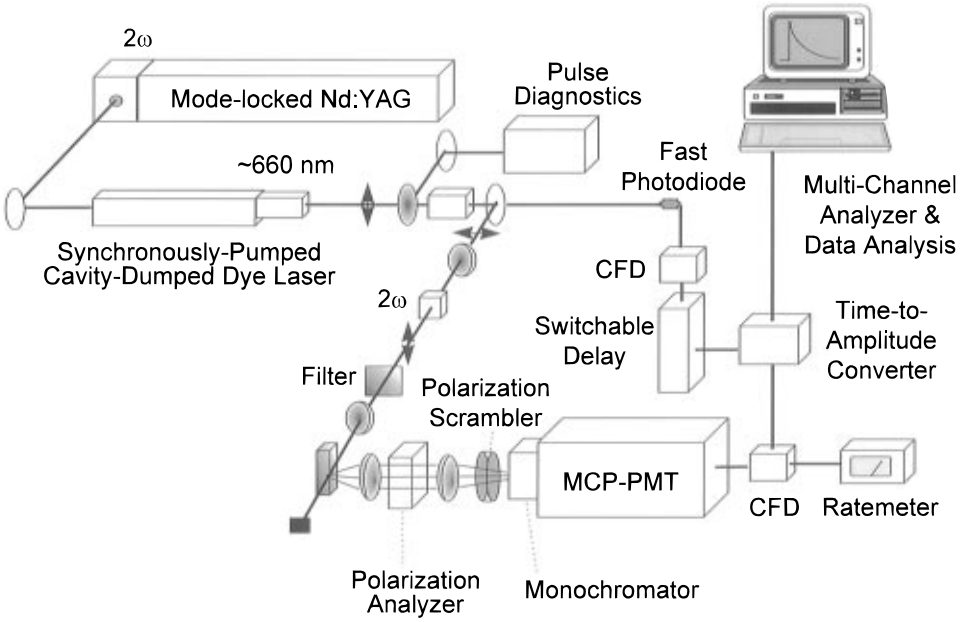

Figure 1. Instrument for TCSPC experiments at The Ohio State University (MCP-PMT = microchannel plate photomultiplier tube, CFD = constant-fraction discriminator). For experiments conducted at Wright-Patterson AFB the dye-laser system was replaced by a mode-locked Ti:sapphire laser, and a pico-timing discriminator replaced the CFD in the MCP-PMT channel.

The decays collected at Wright-Patterson AFB were obtained using a mode-locked Ti:sapphire laser system (Spectra-Physics 3960C-L1S), pumped by an argon ion laser (Spectra-Physics 2080A-25). The 82-MHz output of the Ti:sapphire (1.3 W, 742 nm, 3 ps) was passed through an acousto-optic pulse-picker (Spectra-Physics 3980-5C) to yield a pulse train at 4 MHz (∼55 mW). The laser output was monitored on a 350-MHz oscilloscope (Tektronix 2467) to measure the pulse suppression ratio. By adjusting the pulse-picker, pulse suppression ratios >100 were routinely obtained. After frequency doubling, 3−5 mW of 371-nm radiation was available for excitation, while the residual 742-nm light was directed to the photodiode. In this case, the TCSPC experiment was run in "reverse" mode, with fluorescence photons arriving at the photomultiplier supplying the "start" pulses, and the photodiode pulses serving as the "stop" signals. This configuration minimizes the TAC dead time, since signals are processed only when a fluorescence photon is observed.[32] This is in contrast to the "forward" configuration, in which >99% of the observed "start" pulses have no "stop" pulse associated with them. Pico-timing discriminators were substituted for the CFDs (EG&G Ortec 9307), a GHz preamplifier (EG&G Ortec 9306) replaced the amplifier, and the MCP-PMT was a Hammamatsu R-3809U-01. The MCA employed was a Tennelec/Oxford PCA-Multiport with PCA-III software. The collection optics and other electronic components were identical to those used at The Ohio State University. By utilizing a convolute-and-compare algorithm to fit the data,[33] the TCSPC systems in both laboratories were capable of resolving fluorescence lifetimes on the order of 10 ps.

Results

Absorption and Fluorescence Emission Spectra. The absorption and fluorescence emission spectra of adamantyldiazirine exhibit a well-correlated mirror image relationship (Figure 2). In polar solvents, both spectra experience a red shift and a loss of vibrational structure. Among polar solvents, the absorption spectra in those solvents that are capable of forming hydrogen bonds with the nitrogen lone pairs in adamantyldiazirine's ground state are blue shifted relative to spectra taken in solvents of similar polarity that are not capable of forming hydrogen bonds. For example, the absorption maximum was 372−373 nm in pentane ($\epsilon \sim 245$)[11] and similar hydrocarbons,

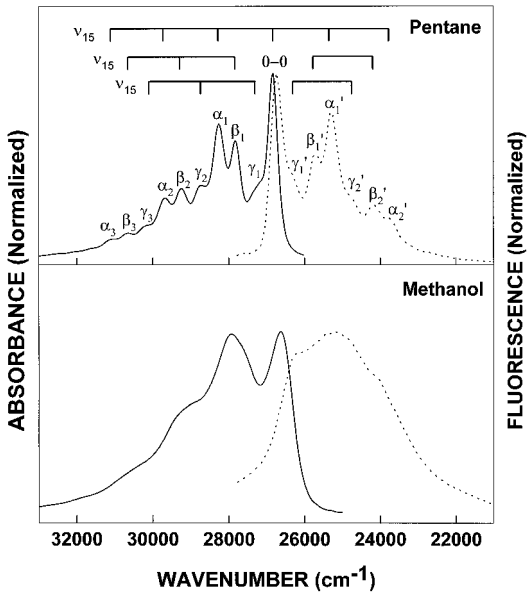

Figure 2. Normalized absorption and fluorescence emission spectra of adamantyldiazirine in pentane and methanol. Peak assignments from PeakFit. Fluorescence excitation was at 355 nm. $A_{335,\text{pentane}} = 0.194$, $A_{335,\text{methanol}} = 0.209$. Solvent Raman bands have been subtracted from the fluorescence spectra.

375−376 nm in methanol and homologous alcohols, and 377 nm in acetonitrile. The peaks that we observed in pentane correspond precisely with those reported by Bayley and Knowles[11] and Morgan.[18] No solvent isotope effect was observed in either the absorption or emission spectra in cyclohexane/cyclohexane-d_{12}, and we observed no changes in the shape of the fluorescence emission spectra when the excitation wavelength was scanned across the absorption band from 330 to 370 nm. Important spectral features are summarized in Table 1. The average fluorescence quantum yield was calculated to be 0.0012 ± 0.0004, and did not vary systematically with solvent. The intensity of fluorescence increased at low temperatures. As the temperature was lowered to 78 K, the emission intensity in methylcyclohexane increased 25-fold relative to ambient temperature. Arrhenius treatment

(32) Nowak, S. A.; Lytle, F. E. *Appl. Spectrosc.* **1991**, *45*, 728−733.
(33) *SPC Software*, Demas, J. N.; Snyder, S. 1989.

Table 1. Solvent Dependence of Absorption Spectrum, Fluorescence Spectrum, Fluorescence Lifetime, Fluorescence Quantum Yield, and Natural Lifetime for Adamantyldiazirine at Ambient Temperature

solvent	absorption bands (nm)[a]	fluorescence bands (nm)[a,b]	comments	τ_F (ns)[c]	ϕ_F	τ_0 (ns)
freon-113	326, 342, 354, 358, *373*	378, 383, 398, 417	broad bands	0.26		
pentane	323, 326, 331, 337, 342, 348, 354, 359, 365, *371, 373*	*374*, 378, 389, 395, 401, 414, 421	highly resolved vibronic structure	0.23	0.0010	237
hexane	337, 341, 348, 354, 359, 366, *373*		highly resolved vibronic structure	0.25		
cyclohexane	322, 326, 332, 338, 342, 349, 355, 360, 366, 372, *373*	*373*, 389, 397, 415	highly resolved vibronic structure	0.23	0.0010	222
cyclohexane-d_{12}	322, 326, 332, 337, 342, 349, 355, 360, 369, *373*, 374	375, 379, 389, 396, 415, 422	highly resolved vibronic structure	0.23		
methanol	328, 342, 358, 362, *376*	380, 393, 405, 416	some structure in absorption spectrum; very broad, featureless fluorescence	0.24	0.0017	140
propanol	326, 344, 357, 362, 370, *375*	377, 387, 391, 399, 411, 428	more structured spectra than methanol	0.25	0.0012	216
butanol	325, 339, 343, 351, 356, 361, 368, 372, *375*	378, 386, 395, 405, 411, 440	more structured spectra than methanol	0.25	0.0016	156
acetonitrile	344, 350, 361, *377*	*386*, 406, 431	very broad, featureless spectra	0.23	0.0009	266

[a] Peaks were assigned based on a fit to a minimum number of Gaussians necessary to yield nonsystematic residuals with the PeakFit software package. The peak responsible for the global maximum of each spectrum is tabulated in italics. Only peaks deemed to be unambiguous contributors to the observed spectrum have been reported. [b] Excitation was at 335 nm. Solvents with C−H bonds exhibited a strong Raman band near 371 nm. To account for this, a spectrum of the pure solvent was collected and the Raman peaks were assigned with PeakFit. The position and width parameter of these peaks were then held constant in the subsequent fits for the diazirine solutions, although the amplitudes were allowed to vary. The Raman bands are not tabulated. [c] Only the lifetime of the major (>80%) component has been tabulated. See text for explanation.

Figure 3. Fluorescence decays for adamantyldiazirine in methylcyclohexane as a function of temperature.

of the fluorescence intensities in this solvent gave an activation energy of 2.90 kcal/mol with a preexponential factor of 2.2×10^{11}.

Fluorescence Lifetime Measurements. This work contains, to the best of our knowledge, the first direct measurements of diazirine fluorescence lifetimes. There was no discernable solvent dependence of the fluorescence lifetime of adamantyldiazirine at ambient temperature. The data were consistently well-described by a single exponential or a sum of two exponentials. The primary decay component fit to a lifetime of 0.24 ± 0.01 ns with no systematic deviation across the range of solvents studied (Table 1). Furthermore, the fluorescence lifetime did not exhibit a solvent isotope effect in cyclohexane/cyclohexane-d_{12}. The fluorescence lifetime data (τ_f) can be related to the natural lifetime of adamantyldiazirine (τ_0) *via* the fluorescence quantum yield (ϕ_f):

$$\tau_0 = \frac{\tau_f}{\phi_f}$$

Using this expression, we estimated the natural lifetime of adamantyldiazirine to be 206 ± 49 ns at ambient temperature. These data are included in Table 1.

A long-lived (0.6−3.2 ns) component was present as a minor contribution to the fluorescence in every solvent (5−31%), although the decays were monoexponential in methylcyclohexane between 173 and 230 K. We attribute this long-lived component to the fluorescence of one or more photoproducts, for reasons that will be addressed later.

The fluorescence lifetime was unaffected by excitation energy. Lifetimes measured with 330-nm excitation were identical to those obtained with 371-nm excitation.

As was true for the fluorescence intensity, decreasing the temperature increased the fluorescence lifetime of adamantyldiazirine. In methylcyclohexane the fluorescence lifetime increased to 7.57 ns at 78 K (Figure 3). In propanol, the lifetime was 8.82 ns at 78 K. Arrhenius treatments of the fluorescence lifetimes in methylcyclohexane and propanol (Figure 4) resulted in activation energies of 2.70 and 2.78 kcal/mol, with preexponential factors of 2.1×10^{11} and 3.5×10^{11}, respectively.

Infrared Spectrum. The infrared spectrum of adamantyldiazirine was obtained in a KBr pellet (Figure 5). Some of the more prominent bands were found at 1570, 1508, 1467, 1450, 1350, 1132, 1080, 1067, and 996 cm^{-1}. Morgan reported a band centered at 1575 cm^{-1} in 3-methylpentane,[18] Bonneau and Liu[16] observed the same peak in isooctane at 1574 cm^{-1}, and

Table 2. Calculated and Experimental Ground State Geometries for Diazirines

	r(N═N)[a]	r(N−C)[a]	θ(NNC)[b]	θ(RCR)[b]	ϕ(NNCR)[b]	μ[c]
diazirine, experiment[39]	1.228	1.482		117.0		1.59
diazirine, SINDO[41]	1.174	1.440	65.9	114.6	105.0	0.47
diazirine, PM3	1.226	1.492	65.7	113.1	105.2	1.87
diazirine, RHF/6-31G* [52]	1.266	1.489		117.0		2.11
diazirine, RHF/6-31G* [4]	1.22	1.50	66.0			
diazirine, MP2/6-31G* [38]	1.256	1.480	64.9	119.4		
dimethyldiazirine, SINDO1[41]	1.166	1.488	66.9	121.3	102.2	0.59
dimethyldiazirine, PM3	1.226	1.501	65.9	115.2	104.5	2.27
adamantyldiazirine, PM3	1.228	1.496	65.8	112.5	105.3	2.50
adamantyldiazirine, B3LYP/6-31G*	1.237	1.477	65.2	113.3	105.4	2.44
adamantyldiazirine, RHF/6-31G*	1.203	1.441	65.3	112.8	105.5	2.62
adamantyldiazirine, MP2(fc)/6-31G*	1.269	1.479	64.6	114.1	105.5	2.85

[a] Distances are in angstroms. [b] Angles are in degrees. [c] Dipole moments are in debye.

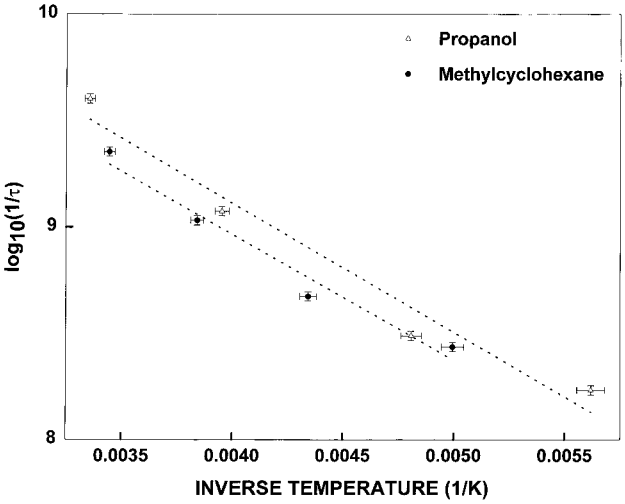

Figure 4. Arrhenius treatment of fluorescence lifetimes for adamantyldiazirine. Calculated activation energies were 2.70 (methylcyclohexane) and 2.78 kcal/mol (propanol). The respective preexponential factors were 2.1×10^{11} and 3.5×10^{11}.

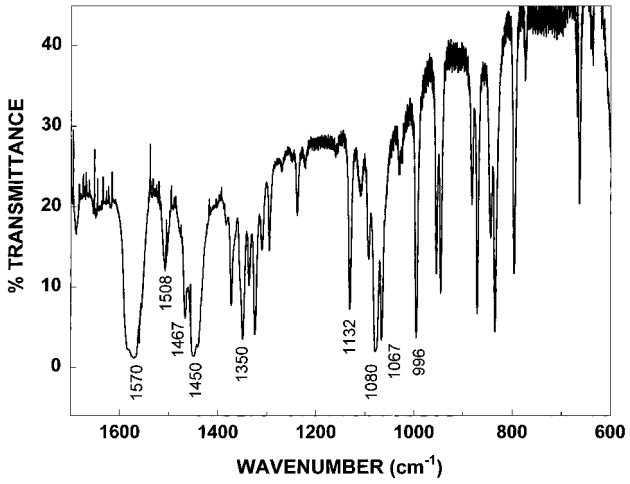

Figure 5. Infrared spectrum of adamantyldiazirine (10 mg) in a 275-mg KBr pellet.

the solution spectrum in $CHCl_3$ has been reported to exhibit peaks at 1540 (with shoulders) and 1450 cm^{-1}.[11] In CCl_4, the strongest band was found at 1550 cm^{-1}.[19]

Semiempirical, ab Initio, and Density Functional Calculations. The PM3 method was used to calculate properties of the ground state and first excited singlet state of adamantyldiazirine. Semiempirical calculations carried out with the PM3 method have been shown to predict successfully a number of experimental observables, including molecular geometries, ionization potentials, and dipole moments.[34,35] Seeger *et al.* have established that vibrational calculations using the PM3 method often provide frequencies and force constants that agree well with experimental values and with those obtained from *ab initio* calculations that require much more intensive computational resources.[36]

To test the appropriateness of the PM3 method for diazirines, we performed a geometry optimization on the ground state of diazirine (H_2CN_2) and compared the results with those obtained from the *ab initio* (6-31G*) calculations of other research groups[4,37,38] (Table 2).

Our PM3 calculation yielded a nitrogen−nitrogen bond length of 1.226 Å, a carbon−nitrogen bond length of 1.492 Å, and an N−N−C bond angle of 65.7°. These values are in excellent agreement with the corresponding *ab initio* values of 1.22 Å, 1.50 Å, and 66.0° obtained by Yamamoto *et al.*[4] Both methods yield geometries that correspond well with the experimentally-determined bond lengths of 1.228 and 1.482 Å obtained from Pierce and Dobyn's analysis of diazirine's microwave spectrum.[39] Encouraged by this result, we performed a similar PM3 calculation on adamantyldiazirine. We found a 1.228-Å nitrogen−nitrogen bond, a 1.496-Å carbon−nitrogen bond, and an N−N−C bond angle of 65.8°. The R−C−R angle at the diazirine carbon was calculated to be 112.5° in adamantyldiazirine, which is nearly identical with the 113.1° angle found for the H−C−H angle in diazirine (PM3). These results suggest that the adamantyl cage has little or no effect on the geometry of the diazirine moiety. When the PM3 method was used to calculate the properties of the lowest excited singlet state (at the ground-state optimized geometry), an expansion of the dipole moment from 2.5 D in S_0 to 3.8 D in S_1* was indicated, consistent with the dipole moment expansion of 1.5 D obtained from the analysis of the Stark spectrum of difluorodiazirine by Lombardi *et al.*[40]

We also performed *ab initio* (RHF/6-31G* and MP2/6-31G*) and density functional (B3LYP/6-31G*) calculations on adamantyldiazirine using the *Gaussian 94* software package. These results are also summarized in Table 2. The calculations were facilitated by the fact that adamantyldiazirine possesses C_{2v} symmetry. At the RHF/6-31G* level the N═N bond was found to be 1.203 Å, the C−N bonds were 1.441 Å, the N−N−C

(34) Stewart, J. J. P. *J. Comput. Chem.* **1989**, *10*, 209−220.
(35) Stewart, J. J. P. *J. Comput. Chem.* **1989**, *10*, 221−264.
(36) Seeger, D. M.; Korzeniewski, C.; Kowalchyk, W. *J. Phys. Chem.* **1991**, *95*, 6871−6879.
(37) Bigot, B.; Ponec, R.; Sevin, A.; Devaquet, A. *J. Am. Chem. Soc.* **1978**, *100*, 6575−6580.
(38) Boldyrev, A. I.; Schleyer, P. v. R.; Higgins, D.; Thompson, C.; Kramarenko, S. S. *J. Comput. Chem.* **1992**, *13*, 1066−1078.
(39) Pierce, L.; Dobyns, S. V. *J. Am. Chem. Soc.* **1962**, *84*, 2651−2652.
(40) Lombardi, J. R.; Klemperer, W.; Robin, M. B.; Basch, H.; Kuebler, N. A. *J. Chem. Phys.* **1969**, *51*, 33−44.

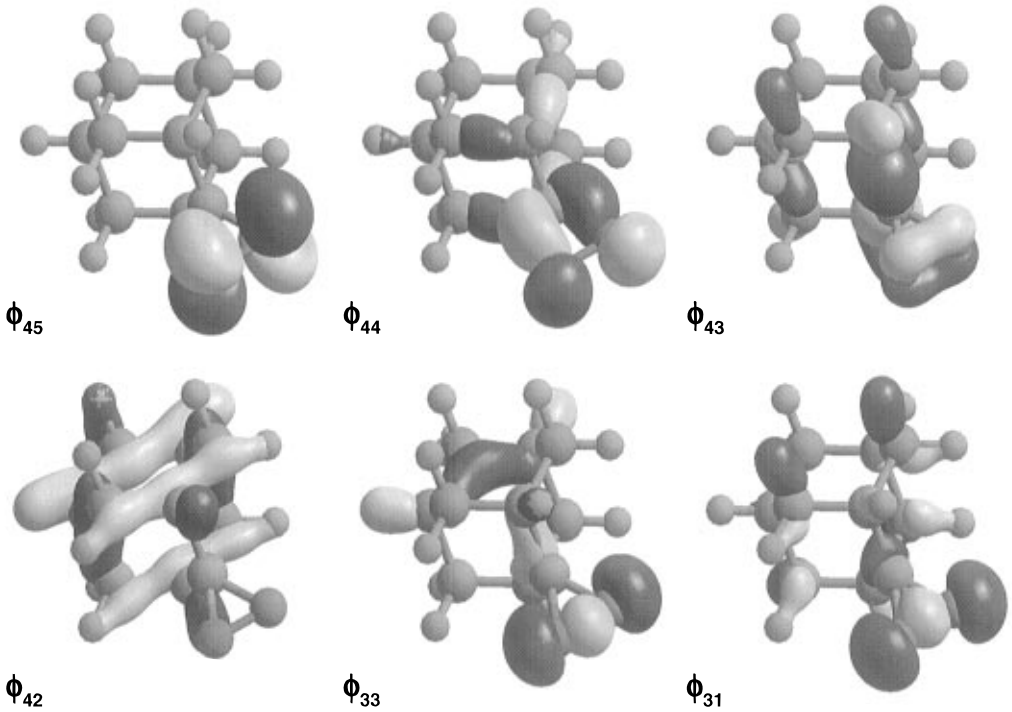

Figure 6. Important molecular orbitals for adamantyldiazirine at the RHF/6-31G* level of theory. Isosurfaces at 0.15 au. Shading indicates the sign of the wavefunction. Orbital numbering is consistent with Table 3.

bond angle was 65.3°, and the R−C−R angle at the diazirine carbon atom was 112.8°. An inspection of some of the significant molecular orbitals of ground-state adamantyldiazirine calculated at this level of theory (Figure 6) confirms that the highest-occupied molecular orbital (ϕ_{44}, HOMO) is nonbonding and antisymmetrical with respect to the nitrogen lone pairs (n$_-$), while the lowest-unoccupied molecular orbital (ϕ_{45}, LUMO) is antibonding, with π^* symmetry. With correction for electron correlation at the second-order Møller−Plesset perturbation (MP2) level, the N═N bond was 1.269 Å, the C−N bonds were 1.479 Å, the N−N−C bond angle was 64.6°, and the R−C−R angle was found to be 114.1°. The B3LYP/6-31G* calculation yielded an N═N distance of 1.237 Å, C−N bond lengths of 1.477 Å, a N−N−C bond angle of 65.2°, and a R−C−R bond angle of 113.3°.

Using the frozen core approximation, a CIS(fc)/6-31G*//MP2-(fc)/6-31G* calculation was performed to examine the *vertical* transitions to the first four excited singlet states. In this context the double slash (//) has its usual meaning to indicate that the calculation was carried out at the MP2(fc)/6-31G* optimized geometry of the ground state. The ground state (singlet) has A_1 symmetry and a calculated dipole moment of 2.62 D along the *z*-axis perpendicular to the N═N bond. The first four excited singlet states were calculated to be of B_1, A_2, B_2, and A_2 symmetries, respectively. Single-photon transitions to the A_2 states are forbidden under C_{2v} symmetry, so only transitions to the first ($f = 0.0016$, *x*-polarized) and third ($f = 0.0421$, *y*-polarized) excited singlet states were predicted to have nonzero oscillator strengths. These vertical transitions were predicted to appear at 3.64 (341 nm) and 7.40 eV (168 nm). The calculation for S_1* agrees well with the experimental absorption spectrum of adamantyldiazirine, measured in pentane. Its origin appears at 3.32 eV (373 nm).

Interestingly, each of the first four vertical transitions terminates in the same π^* unoccupied molecular orbital (ϕ_{45}, LUMO), but the dominant CI excitations for each transition (Table 3) correspond to excitations from different combinations of occupied molecular orbitals. These differences are illustrated in the charge density difference plots provided in Figure 7, where the solid lines correspond to charge accumulation in the excited state and dashed lines correspond to charge depletion from the ground state. Figure 7 (top) shows that the first two vertical excited states accumulate charge density in a similar spatial region (π^*), but Figure 7 (bottom) shows that the two states deplete charge density from very different areas. In the transition to S_1* ($1B_1$), a considerable amount of electron density is taken from the lone-pair region in "front" of the nitrogens on the diazirine ring. Additional electron density is drawn from the entire adamantyl cage. The transition to S_2* ($1A_2$), in contrast, depletes the lone-pair region to the "sides" of the nitrogens in the diazirine ring and takes very little electron density from the far side of the adamantyl cage. The transitions

Table 3. CIS(fc)/6-31G* Vertical Transitions for Adamantyldiazirine at the MP2/6-31G* Ground-State Optimized Geometry

	transition energy[a]	transition wavelength[b]	orbitals (coefficients)	μ of final state[c]
S_0 ($1A_1$), C_{2v}				2.62
S_1* ($1B_1$), C_{2v}	3.64	341	36 → 45 (+0.13) 41 → 45 (−0.22) 44 → 45 (+0.65)	4.26
S_2* ($1A_2$), C_{2v}	6.81	182	31 → 45 (+0.38) 33 → 45 (+0.46) 37 → 45 (−0.32) 42 → 45 (−0.10)	3.31
S_3* ($1B_2$), C_{2v}	7.40	168	35 → 45 (+0.19) 40 → 45 (−0.35) 43 → 45 (+0.52)	4.43
S_4* ($2A_2$), C_{2v}	9.29	133	23 → 45 (+0.11) 24 → 45 (+0.21) 25 → 45 (+0.29) 26 → 45 (−0.15) 31 → 45 (+0.30) 37 → 45 (+0.29) 42 → 45 (+0.38)	5.11

[a] Transition energies are in eV. [b] Transition wavelengths are in nanometers. [c] Dipole moments are in debye.

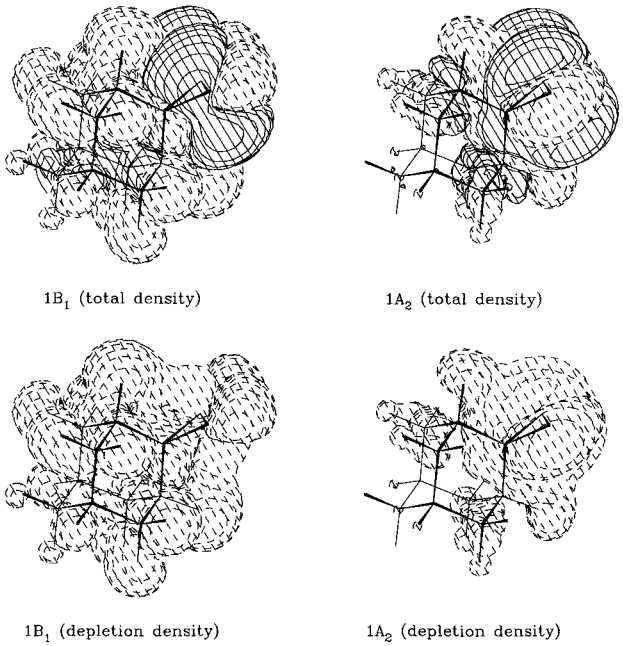

Figure 7. Charge density difference plots and charge density depletion plots for going from the ground state to the first two vertical excited states in adamantyldiazirine. The contour level is 1.0×10^{-4} e/B^3. Solid contours correspond to regions of increased electron density in the excited state, while dashed regions correspond to depleted regions from the ground state.

Table 4. CIS(fc)/6-31G* Optimized Structures and Energies for Ground and Excited Singlet States of Adamantyldiazirine

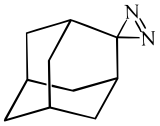

	S_0	S_1*		S_2*	S_3*
	($1A_1$), C_{2v}	($1B_1$), C_{2v}	($1A''$), C_s	($1A_2$), C_{2v}	($1B_2$), C_{2v}
r(N═N)[a]	1.203	1.249	1.264	1.531	1.491
r(N−C)[a]	1.441	1.494	1.386 1.652	1.417	1.345
θ(NNC)[b]	65.3	65.3	54.8 77.0	57.3	56.4
θ(RCR)[b]	112.8	114.5	114.3	111.7	106.7
ϕ(NNCR)[b]	105.5	105.0	98.6 110.2	110.1	112.4
NIMAG[c]	0	1	0	1	
ΔE[d]		3.83	3.77	5.88	6.09

[a] Distances are in angstroms. [b] Angles are in degrees. [c] Number of imaginary vibrational frequencies. [d] ΔE is the difference in energy (eV) between the ground and excited states, without ZPE correction.

to S_3* and S_4* (not shown) are less easily summarized, but they appear qualitatively similar to the transition to S_1* in that they draw more from the "front" of the nitrogens than from the "sides".

Attempts to optimize the geometries of the S_1* ($1B_1$) state did not locate a minimum within C_{2v} symmetry. Instead, the optimum C_{2v} geometry corresponded to a transition state. Similarly, the S_2* state, which is $1A_2$ under C_{2v} symmetry, also yielded a transition state rather than an energy minimum in its optimized C_{2v} geometry. Our calculations showed that the state ordering and energies are extremely sensitive to the geometry changes that lead to these transition states. The CIS(fc)/6-31G* optimized geometries are given in Table 4.

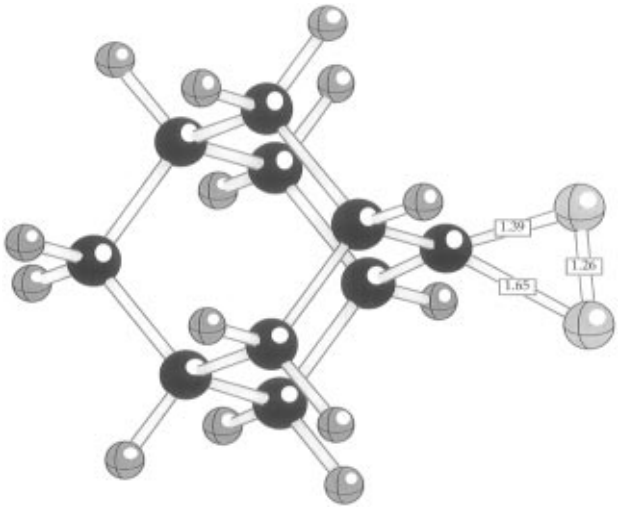

Figure 8. Optimized geometry (CIS/6-31G*, C_s symmetry) for the $1A''$ (S_1*) state of adamantyldiazirine. The mirror plane containing the diazirine ring is retained when C_{2v} symmetry is reduced to C_s.

To explore the reaction surface further, we nudged both of the transition states ($1B_1$ and $1A_2$) along the normal coordinates of their transition state frequencies and optimized their geometries under the resulting C_s symmetry. The mirror plane containing the diazirine ring was retained in both cases, but the other mirror plane was broken. In C_s, both states possessed A'' symmetry and converged on the *same* minimum geometry (Table 4, Figure 8). Mixing of these two states (forbidden by symmetry in C_{2v}) was made possible when the symmetry was reduced to C_s. The implications for adamantyldiazirine's photochemistry are discussed below.

Our calculated ground-state geometries seem quite reasonable in comparison with published results for smaller diazirines. They agree well with experimental studies of difluorodiazirine by Lombardi *et al.*,[40] semiempirical calculations (SINDO1) for diazirine and 3,3-dimethyldiazirine by Müller-Remmers and Jug,[41] and studies for diazirine with the *ab initio* calculations of Yamamoto *et al.*, Devaquet *et al.*, and Boldyrev *et al.*[4,37,38] Pictures of the frontier molecular orbitals of adamantyldiazirine, calculated semiempirically with the AM1 method, have been published by Morgan.[18] We note that the orbitals look very similar to those discussed here.

To assist with the interpretation of the absorption, fluorescence, and infrared spectra, we performed semiempirical (PM3), *ab initio* (RHF/6-31G*), and density functional (B3LYP/6-31G*) vibrational analyses on the $1A_1$ (C_{2v}), $1B_1$ (C_{2v}), $1A_2$ (C_{2v}), and $1A''$ (C_s) states of adamantyldiazirine with *Gaussian 94*. The 72 ground-state fundamental vibrations and their symmetry assignments under C_{2v} are $22a_1$ ($\nu_1-\nu_{22}$), $14a_2$ ($\nu_{23}-\nu_{36}$), $18b_1$ ($\nu_{37}-\nu_{54}$), and $18b_2$ ($\nu_{55}-\nu_{72}$). These are available in tabular form in the Supporting Information. Our calculations indicate that the N═N stretching mode (ν_{17}) is unique among adamantyldiazirine's a_1 modes in that it experiences a major frequency reduction upon excitation to S_1*. Its RHF/6-31G* frequency in the C_s-optimized geometry of S_1* is 260 cm^{-1} lower than that of the C_{2v}-optimized ground state. Most of the other modes shift by only a few wavenumbers.

Discussion

The absorption, fluorescence, and infrared spectra of adamantyldiazirine provide information about its ground- and excited-state structures. We begin our discussion by examining

(41) Müller-Remmers, P. L.; Jug, K. *J. Am. Chem. Soc.* **1985**, *107*, 7275−7284.

the vibrational assignments for the ground and excited states. We compare our experimental results with semiempirical, *ab initio*, and density functional calculations to analyze the geometries, fundamental vibrations, and electron density distributions of these states. We then discuss the fluorescence lifetime data. The fluorescence lifetime serves as a probe of the dynamics of the excited state, and its temperature and solvent dependence provide indirect access to the rates of the competing excited-state decay processes. We discuss the implications of our data with regard to the relative contributions of *inter*- and *intra*molecular processes in the excited state photochemistry of adamantyldiazirine.

Vibrational Assignments. By comparing the infrared spectrum (Figure 5) with the calculated normal modes of adamantyldiazirine and the vibrational assignments for diazirine (H_2CN_2) and 3,3-dimethyldiazirine tabulated by other research groups[42,43] it is clear that the strong band observed in the infrared spectrum at 1570 cm^{-1} can be assigned to ν_{17}, a mode that is best described as an N═N stretch, although it also includes a contribution from an R−C−R scissoring motion on the diazirine carbon. This vibration has a_1 symmetry under C_{2v}. Calculations at the PM3, B3LYP/6-31G*, and RHF/6-31G* levels overestimated the frequency of this vibration by at least 135 cm^{-1}. We performed similar calculations for diazirine, 3-methyldiazirine, 3,3-dimethyldiazirine, and 3,3-difluorodiazirine. In each case, the calculated N═N stretching frequency was higher than the reported experimental values.[42−45] In order to obtain satisfactory agreement with experimental values for these smaller diazirines, vibrational analyses at the MP2/6-31G* level were required. We expect that an MP2/6-31G* vibrational analysis would also successfully model ν_{17} for adamantyldiazirine, but we were unable to perform such a large calculation with our current resources. We estimate that about 16 GB of disk space would have been required. While the MP2/6-31G* vibrational analysis proved to be unwieldy, we were able to optimize the geometry of adamantyldiazirine at the MP2/6-31G* level. For small diazirines, the MP2/6-311G* frequency of the N═N stretch exhibited a nearly linear inverse dependence on the calculated MP2/6-31G* N═N bond length. If this simple correlation can be extended to adamantyldiazirine, we would expect the 1.269 Å calculated N═N bond length (Table 2) to correspond to an MP2/6-31G* stretching frequency of ∼1563 cm^{-1}, in excellent agreement with the 1570-cm^{-1} band observed in the infrared spectrum. While our data are not currently capable of unambiguously assigning the remainder of the infrared spectrum, we tentatively suggest (on the basis of calculated band positions and infrared intensities) that the 1508-cm^{-1} band arises from ν_{16} (a_1) while the bands at 1467 and 1450 cm^{-1} arise primarily from ν_{15} (a_1), ν_{50} (b_1), and ν_{69} (b_2).

The mirror image relationship between the absorption and emission spectra (Figure 2) of adamantyldiazirine proves that the fluorescent species is adamantyldiazirine rather than an impurity, and its structure is consistent with the molecule's rigid geometry.[8] It confirms a non-zero oscillator strength for the $S_1^* \leftarrow S_0$ absorption, and indicates that the vibrational spacings in S_1^* are similar to those of S_0. In pentane, where the vibrational structure is well-resolved, our data seem to justify a preliminary assignment of several bands (Table 5). The most prominent fluorescence bands appear at 374 and 395 nm, respectively. There is another sharp band between them at 389 nm, although it is less intense than the band at 395 nm. A broader band at 378 nm appears as a shoulder to the 374-nm band. The mirror image bands in the absorption spectrum occur at 373 (most intense), 369 (shoulder), 359 (sharp), and 354 nm (sharp, strong). A satisfying interpretation may be obtained by taking the most intense band in each spectrum as 0−0 and using the spacings to the next three bands as vibronic origins. We have labeled these vibronic origin bands as α_1, β_1, and γ_1 in the absorption spectrum and as α_1', β_1', and γ_1' in the fluorescence emission spectrum. In the fluorescence spectrum these spacings correspond to 1460 (α_1'), 1033 (β_1'), and 334 cm^{-1} (γ_1'). There are several ground-state normal modes of adamantyldiazirine with calculated frequencies very close to these values. In fact, only a few of these modes need to be considered, as the vibrational structure of the absorption band must involve totally symmetric (a_1) vibrations.[30] Therefore, using the RHF/6-31G* scaled frequencies, the most likely possibilities are ν_1 (319 cm^{-1}), ν_8 (1002 cm^{-1}), ν_9 (1080 cm^{-1}), ν_{15} (1458 cm^{-1}), and ν_{16} (1483 cm^{-1}). From the infrared spectrum, we know that adamantyldiazirine has strong, sharp bands at 1067, 1080, 1450, and 1467 cm^{-1}. The vibronic spacings in the absorption spectrum are quite similar to their counterparts in the emission spectrum: 1429 cm^{-1} (α_1), 1008 cm^{-1} (β_1), and 289 cm^{-1} (γ_1). This mirror image relationship is consistent with the results of our CIS(fc)/6-31G* calculations (Table 4) that predict very slight changes in the molecular geometry upon excitation to S_1^*. The lack of a Stokes shift and the mirror image between the spectra also supports the conclusion that S_1^* is $1B_1$ rather than $1A_2$, since A_2 states should have zero oscillator strength under C_{2v}. The scaled CIS(fc)/6-31G* frequencies for the $1B_1$ state are ν_1 (318 cm^{-1}), ν_8 (1001 cm^{-1}), ν_9 (1077 cm^{-1}), ν_{15} (1458 cm^{-1}), and ν_{16} (1484 cm^{-1}). These values are essentially unchanged relative to their ground-state counterparts.

We note that there is some uncertainty in these assignments, arising from the width of the vibronic bands in the solution-phase absorption and emission spectra at room temperature. Nevertheless, our assignments are supported by the remaining peaks in the absorption and fluorescence spectra. For example, the absorbance band at 354 nm (α_1, 15_0^1) initiates a series of harmonics, spaced by ∼1429 cm^{-1}, that appear at 337 (α_2, 15_0^2) and 321 nm (α_3, 15_0^3). The mirror image bands in the fluorescence spectrum, spaced by ∼1460 cm^{-1}, appear at 395 (α_1', 15_1^0) and 421 nm (α_2', 15_2^0). This last band is rather weak and is largely submerged beneath the fluorescence envelope, so it is not surprising that its frequency is a somewhat poor

Table 5. Transition Frequencies (cm^{-1}) and Assignments for Adamantyldiazirine in Pentane

band	ν	$\Delta\nu$	assignment
absorption spectrum	26824	0	0−0 origin
α_1	28253	1429	15_0^1
α_2	29687	2863	15_0^2
α_3	31104	4280	15_0^3
β_1	27832	1008	8_0^1
β_2	29252	2428	$8_0^1 15_0^1$
β_3	30686	3862	$8_0^1 15_0^2$
γ_1	27113	289	1_0^1
γ_2	28732	1909	$1_0^1 15_0^1$
γ_3	30183	3359	$1_0^1 15_0^2$
fluorescence emission spectrum	26758	0	0−0 origin
α_1'	25298	1460	15_1^0
α_2'	23773	2985	15_2^0
β_1'	25725	1033	8_1^0
β_2'	24172	2586	$8_1^0 15_1^0$
γ_1'	26424	334	1_1^0
γ_2'	25006	1752	$1_1^0 15_1^0$

(42) Gambi, A.; Winnewisser, M.; Christiansen, J. J. *J. Mol. Spectrosc.* **1983**, *98*, 413−424.
(43) Mitchell, R. W.; Merritt, J. A. *J. Mol. Spectrosc.* **1968**, *27*, 197−209.
(44) Simmons, J. D.; Bartky, I. R.; Bass, A. M. *J. Mol. Spectrosc.* **1965**, *17*, 48−49.
(45) Sieber, H.; Bruno, A. E.; Neusser, H. J. *J. Phys. Chem.* **1990**, *94*, 203−208.

match. The vibronic origin at 359 nm (β_1, 8_0^1) initiates a *progression* of bands in ν_{15} that appear at 342 (β_2, $8_0^1 15_0^1$) and 326 nm (β_3, $8_0^1 15_0^2$). The corresponding bands in the fluorescence spectrum appear at 389 (β_1', 8_1^0) and 414 nm (β_2', $8_1^0 15_1^0$). Again, the uncertainty in the position of this last band is considerable. Finally, the vibronic origin at 369 nm (γ_1, 1_0^1) also initiates a progression in ν_{15} to 348 (γ_2, $1_0^1 15_0^1$) and 331 nm (γ_3, $1_0^1 15_0^2$). In this case, there is some uncertainty in the position of all three bands. The mirror image bands appear at 378 (γ_1', 1_1^0) and 400 nm (γ_2', $1_1^0 15_1^0$) in the fluorescence spectrum.

Vibrational frequencies tend to decrease slightly in excited states relative to their corresponding ground state frequencies. Our assignments (Table 5) and CIS(fc)/6-31G* calculations reflect this. As mentioned previously, only the N═N stretching mode is predicted to experience a significant shift in frequency ($\Delta\nu = -260$ cm^{-1}) upon excitation to S_1*. We note that if the N═N stretch ($\sim$1570 cm^{-1} in the ground state infrared spectrum) contributes to the vibronic structure in the absorption and emission spectra, it does so only weakly, as none of the stronger bands in the absorption or emission spectra exhibit spacings of this magnitude. This was also observed for diazirine (H_2CN_2).[46] On the other hand, when Lombardi *et al.*[40] investigated 3,3-difluorodiazirine (F_2CN_2), they observed a long progression in the N═N stretch. The difference in behavior between diazirine and 3,3-difluorodiazirine was explained by appealing to the fact that the HOMO in ground state diazirine contains 50% more density on the carbon atom than the same orbital in 3,3-difluorodiazirine. This is a consequence of the electron-withdrawing nature of fluorine relative to hydrogen. Carbon−nitrogen bonding is therefore more important in the HOMO of diazirine than in the HOMO of 3,3-difluorodiazirine. This causes the subsequent $^1(n_- - \pi^*)$ excitation in diazirine to be weighted more toward a lengthening of a C−N bond rather than a lengthening of the N═N bond. As alkyl groups tend to be electron donating, our observation of a progression in a C−N mode (ν_{15}) rather than the N═N mode (ν_{17}) in adamantyldiazirine is consistent with their interpretation. Our *ab initio* calculations predicted a significant deformation of the diazirine ring in S_1* as the molecule moves from C_{2v} to C_s symmetry (Figure 8). This deformation is accompanied by a large reduction in the frequency of the N═N stretch. The reduced symmetry allows the N═N stretch to mix with several of the CH_2 scissoring modes of the adamantyl cage. This also helps to explain the absence of the N═N stretch from the vibronic structure. Under these conditions it is reasonable to expect a relatively small Frank-Condon overlap for this mode, giving rise to weak vibronic coupling. All of these results are consistent with our CIS(fc)/6-31G* calculation of the vertical transition to S_1* ($1B_1$). This excitation involves promotion of an electron primarily from an n_- orbital (ϕ_{44}) into an antibonding π* orbital (ϕ_{45}). This weakens the bond between the nitrogens, reducing the force constant of the vibration. The frequency reduction that results from the weaker force constant makes this mode roughly isoenergetic with CH_2 scissoring vibrations in the adamantyl cage, and these modes mix under C_s symmetry.

We note that these results are consistent with those found for F_2CN_2 by Lombardi *et al.*, Simmons *et al.*, and Sieber *et al.*[40,44,45]

Excitations, Excited States, and Photochemistry. The observed red shifts in the steady-state absorption and fluorescence spectra with increasing solvent polarity indicate that the excited state of the diazirine is more polar than the ground state and that the excited state (S_1*) interacts more strongly than the ground state (S_0) with more polar solvents. This is consistent with the results of our *ab initio* and semiempirical calculations that indicate an increase in dipole moment upon excitation that can be attributed to a localization of electron density on the diazirine nitrogens in S_1*. This interpretation also explains the red shift of the spectra in CH_3CN relative to solvents of similar polarity that are capable of forming hydrogen bonds with the nitrogen lone pairs in S_0. Hydrogen bonding solvents would be expected to stabilize the ground state more than the $^1(n_- - \pi^*)$ excited state, so the energy gap between the states is expected to be larger under these circumstances. It is not surprising that this is a weak effect, however, as Haselbach *et al.* found that the two electrons in the n_- antisymmetric "lone pair" molecular orbital of 3,3-dimethyldiazirine are only 56% localized on the two nitrogen atoms.[47]

We believe that the fluorescence of adamantyldiazirine originates from the lowest excited singlet state, S_1*, since neither the structure of the fluorescence emission spectrum nor the fluorescence lifetime displayed a dependence upon excitation wavelength. The observed mirror image relationship between the absorption and fluorescence spectra lends further support to this conclusion.

Our data appear to be largely consistent with the current theoretical understanding of the reactivity of diazirines and alkyl-substituted diazirines. The general scheme, initially developed at the semiempirical level by Müller-Remmers and Jug,[41] has recently been mapped out in more detail and extended with *ab initio* MC-SCF methods by Yamamoto *et al.*[4] Specifically, excitation at the red edge of the absorption spectrum creates an $^1(n_- - \pi^*)$ state that can, in principle, decay by a variety of pathways. For diazirine (H_2CN_2) three nonradiative decay processes have been identified.[4] The most straightforward of these involves isomerization to diazomethane *via* a conical intersection at a bent-in-plane (bip), diazomethane-like diradicaloid structure. A very slight (0.55 kcal/mol) barrier must be surpassed to initiate this reaction from the S_1* minimum. A second pathway arises from vibrational leakage from the first pathway, across a bifurcation point on the S_1* surface, along a bent-out-of-plane (bop) pathway to a second conical intersection at a ring-opened diazirine diradicaloid structure. Movement through this funnel leads to the formation of a carbene and molecular nitrogen. A third possibility involves thermal population of S_2* from the S_1* surface. The S_0 product surface is then accessed *via* the same conical intersection employed by the second pathway, to yield nitrogen and singlet carbene. Intersystem crossing to a triplet state is not expected to contribute significantly to the depopulation of S_1*,[4] and this has been confirmed experimentally by Modarelli *et al.* for 3-methyldiazirine and 3,3-dimethyldiazirine.[5,48] Seburg and McMahon reached the same conclusion for 3-methyldiazirine.[49]

We note that diazirine's S_2* state has been assigned as $^1(n_- - \sigma^*)$ by Yamamoto *et al.*,[4] but our CIS(fc)/6-31G* calculations on adamantyldiazirine indicate that transitions to each of its first four excited singlet states terminate primarily in the LUMO, which has π* character. This was noted previously in our discussion of the charge density difference plots in Figure 7. We believe that the first few excited states of adamantyldiazirine should be adequately defined at this level of theory. We have calculated the first six CIS vertical excited states at the MP2-

(46) Robertson, L. C.; Merritt, J. A. *J. Mol. Spectrosc.* **1966**, *19*, 372−388.

(47) Haselbach, E.; Heilbronner, E.; Mannschreck, A.; Seitz, W. *Angew. Chem.* **1970**, *9*, 902−903.

(48) Modarelli, D. A.; Platz, M. S. *J. Am. Chem. Soc.* **1993**, *115*, 470−475.

(49) Seburg, R. A.; McMahon, R. J. *J. Am. Chem. Soc.* **1992**, *114*, 7183−7189.

(fc)/6-31G* geometry for diazirine (H_2CN_2) using several basis sets. The energies of these states are tabulated in the Supporting Information. We found that the excited state ordering is identical for the first three excited states for all four basis sets employed (6-31G*, 6-31+G*, 6-311++G**, and 6-31+G*R) and the energies of these states change very little as the basis set is improved. These results suggest that the spatial distribution of the first three excited states should be reasonably well-described at the 6-31G* level. The CIS(fc)/6-31G* state orderings for the first four excited states of adamantyldiazirine are identical to those calculated at the CIS(fc)/6-31G* level for diazirine, and the energies of these states are also quite similar. Therefore, we would not expect our results for adamantyldiazirine to be significantly improved with a larger basis set.

The extent to which adamantyldiazirine's photochemistry resembles that of diazirine is unclear. Most alkyl- and dialkyldiazirines possess α-hydrogens that have been postulated to migrate either concurrent with or subsequent to nitrogen extrusion to generate alkenes.[50] The α-hydrogens of adamantyldiazirine are not expected to undergo these rearrangements, as the rigid adamantyl cage strongly inhibits the formation of internal double bonds. With these rearrangement pathways blocked, the options available to a photoexcited molecule of adamantyldiazirine are nearly identical to those open to diazirine itself: internal conversion, fluorescence, intersystem crossing, carbene formation, and rearrangement to form a diazo compound. Adamantyldiazirine has also been shown to undergo an *intra*molecular insertion reaction under certain conditions (usually at temperatures >200 °C) to form the highly strained 2,4-dehydroadamantane,[13,17−19] but to our knowledge this product has never been observed to account for more than ∼7% of the product distribution in photochemical experiments conducted at ambient temperature in any of the solvents employed in our investigations.[13,18]

Since our experiments were carried out in solution, *inter*molecular chemistry was also a possibility. While the possible decay pathways are therefore quite similar to those in diazirine, there are enough differences between the two species to anticipate that the topologies of the reaction surfaces in the excited state might be somewhat different, leading to unequal partitioning among the possible decay pathways. For example, the electron-donating nature of the adamantyl cage could stabilize pathways such as carbene formation. On the other hand, reaction pathways that involve dramatic changes in the molecular geometry might be more hindered in adamantyldiazirine than in the more flexible diazirine. Consequently, it would be unwise to expect the reaction surface mapped out by Yamamoto *et al.*[4] to apply equally well to adamantyldiazirine. Recent experiments conducted by Bonneau and Liu[16] in isooctane solutions of adamantyldiazirine suggest that the photochemistry partitions in approximately equal ratios to form 2-diazoadamantane and adamantylidene.

The increases in fluorescence intensity and fluorescence decay time observed at low temperatures confirm that fluorescence competes with at least one activated chemical process in adamantyldiazirine's excited state. Arrhenius treatments of these data yielded activation energies of 2.7−2.9 kcal/mol (Figure 4). This energy corresponds to the lowest (*i.e.*, rate-limiting) barrier on the excited state (S_1*) surface. There was good agreement between activation parameters obtained from the steady-state fluorescence intensities and those derived from the fluorescence lifetimes. The calculations of Yamamoto *et al.*[4] found a rate-limiting barrier of 0.55 kcal/mol for the isomerization of diazirine to diazomethane. While they were unable to locate a transition state along a pathway leading to carbene, they were able to establish a maximum barrier of this process of 4 kcal/mol. Müller-Remmers and Jug also predicted a barrier of a few kilocalories per mole for the analogous process in dimethyldiazirine,[41] so our range of 2.7−2.9 kcal/mol for adamantyldiazirine seems quite reasonable. It confirms our intuitive sense that the photochemistry ought to be somewhat more hindered in adamantyldiazirine relative to diazirine due to the rigid molecular architecture, but not prohibitively so, as the diazirine moiety is identical in both systems.

Our CIS(fc)/6-31G* explorations of the excited state surfaces of adamantyldiazirine lend further support to these conclusions. Neither S_1* nor S_2* exhibited minima under C_{2v} symmetry. Both of the states become A″ symmetric under C_s when the mirror plane containing the diazirine ring is retained. Consequently, mixing of the states (which was symmetry forbidden in C_{2v}) is possible under C_s. Both states converge to the *same* optimum geometry under these circumstances. We obtained identical results for diazirine (H_2CN_2) at the CIS(fc)/6-31G*, CIS(fc)/6-31+G*, and the CIS(fc)/6-311++G** levels of theory. In every case (for diazirine and adamantyldiazirine) the optimized C_s structure possesses a lengthened (1.65−1.66 Å) and a shortened (1.37−1.39 Å) carbon−nitrogen bond. Our data do not map out a complete photochemical reaction surface for adamantyldiazirine, but the optimized C_s structure is consistent with the formation of 2-diazoadamantane *via* a bent-out-of-plane mechanism. This seems to support the conclusions drawn from the experimental work of Bonneau and Liu.[16] We note, however, that our results are at variance with the MC-SCF (6-31G*) calculations of Yamamoto *et al.*[4] in which the S_1* and S_2* states of diazirine possessed minima under C_{2v} symmetry and the photochemical conversion to diazomethane was described as a surface-crossing mechanism *via* a conical intersection along an asymmetric (C_1) bent-out-of-plane pathway.

Since neither the fluorescence lifetime nor the steady-state fluorescence spectrum exhibited a solvent isotope effect, the abstraction of hydrogen atoms from the solvent by the diazirine excited state does not appear to be a process that competes significantly with fluorescence. In fact, the lack of any solvent dependence on the room temperature fluorescence lifetime of adamantyldiazirine suggests that the solvent does not play a crucial role in determining the rates of any activated processes that compete with fluorescence in the diazirine excited state. We conclude that any solvent-insertion processes that do occur[13] are attributable to chemistry of subsequent intermediates (*e.g.*, adamantylidene or 2-diazoadamantane), and not that of the diazirine excited state. The lack of a solvent dependence or noticeable oxygen dependence for the fluorescence lifetime also seems to be inconsistent with the hypothesis that exciplexes of certain solvents or triplet oxygen ($^3O_2$) with the excited state of adamantyldiazirine might be responsible for some of the observed photochemistry.[13]

Photoproducts. We attribute the minor component of the fluorescence decays to luminescent photoproducts. None of the solvents exhibited significant fluorescence, and the relative contribution of the long-lived decay component seemed to depend only upon the amount of time a given sample had spent in the laser beam. While we are unable to discount completely the possibility that this minor component had its origin in relevant photophysical processes of adamantyldiazirine, it would be difficult to explain the observed reproducibility of the major (0.24 ns) component and the variability of the minor component simultaneously. For example, the minor component had a lifetime of 0.57 ns in pentane, but in hexane the lifetime jumped

(50) Platz, M. S.; White, W. R.; Modarelli, D. A.; Çelebi, S. *Res. Chem. Intermed.* **1994**, *20*, 175−193.

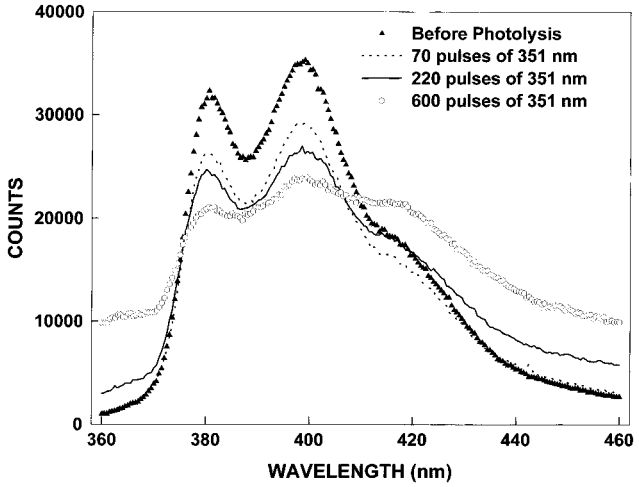

Figure 9. Fluorescence emission spectra of adamantyldiazirine in Freon-113 indicating the effect of photolysis using a pulsed XeF excimer laser (351 nm, 60 mJ/pulse, 17 ns/pulse).

Table 6. Emission-Wavelength Dependence of Adamantyldiazirine's Fluorescence Lifetime in Freon-113

emission λ (nm)	τ_1 (ns)	τ_2 (ns)	% τ_1	% τ_2
390	0.27	3.2	93	7
400	0.26	2.7	94	6
420	0.30	3.1	82	18
390 (after photolysis)	0.36	2.4	31	69

to 1.0 ns. Similarly, the minor component was responsible for 31%, 9%, and 18% of the decay in methanol, propanol, and butanol, respectively. The collection times for these samples (a very rough measure of the extent of photolysis) were 4761, 1800, and 3458 s, respectively. Photoproduct fluorescence was also indicated in steady-state emission spectra measured in Freon-113 (Figure 9). A broad, featureless fluorescence with a maximum at 416 nm replaced the more structured spectrum due to adamantyldiazirine (emission maximum at 398 nm) as the sample was subjected to 600 intense pulses of 351-nm radiation from an XeF excimer laser.

Additional support for attributing the long-lived component to photoproduct fluorescence comes from the emission wavelength dependence of the fluorescence lifetimes (Table 6). In Freon-113, there were negligible changes in the relative contributions of the two decay components as the emission wavelength was varied near the maximum for adamantyldiazirine (390−400 nm), but when the decay was monitored at 420 nm (near the emission maximum of the photoproduct(s)) the relative contribution of the long-lived species increased from 6% to 18%. When the sample was subjected to extensive 350-nm photolysis, the contribution of the long-lived component reached 69%, even when monitored at 390 nm. Among the photoproducts that have been observed previously,[3,13,16,18] adamantanone and adamantanone azine possess chromophores that would make them possible sources of the long-lived fluorescence. It is possible, however, that the species responsible for the fluorescence is formed in microscopic quantities and has gone undetected in previous analyses, owing to the extreme sensitivity of fluorescence techniques relative to other methods such as gas chromatography.

Conclusions

The fluorescence lifetime of adamantyldiazirine was measured using the time-correlated single-photon counting technique and found to be on the order of 240 ps at ambient temperature. To our knowledge, this is the first such measurement to be reported in the literature for a diazirine. Our Arrhenius treatment of the temperature dependence of the fluorescence provides experimental support for the calculations of previous groups that predicted a barrier to carbene and/or diazo formation on the S_1* surface of diazirines.[4,37,41,51] For adamantyldiazirine, this value was determined to be between 2.7 and 2.9 kcal/mol.

Our CIS calculations did not find energy minima for the S_1* and S_2* states under C_{2v} symmetry for diazirine or adamantyldiazirine. Previous calculations at the MC-SCF/6-31G* level found a shallow minimum for the S_1* state under C_{2v}.[4] Furthermore, while our calculations are consistent with photoisomerization of diazirines to diazo compounds, we have found a potential intermediate at a C_s geometry (retaining the mirror plane containing the diazirine ring) that corresponds to an energy minimum on both the S_1* ($1B_1$) and S_2* ($1A_2$) surfaces. Our data therefore allow for a simple mixing between these states, without appealing to the S_1*/S_2* conical intersection indicated in the MC-SCF calculations.[4]

There are at least two possible reasons for the different structures and mechanism found by the two computational methods. The CIS method ignores excitations above singles, so it might not treat higher excited states (*e.g.*, S_2*) as adequately as does the MC-SCF approach. On the other hand, the success of the MC-SCF method depends on the choice of the "active space" under consideration. For example, the calculations of Yamamoto *et al*. employed an active space of six electrons in six active orbitals.[4] Our CIS calculations reveal that a significant contribution to the S_1* state involves an excitation from ϕ_{41} (HOMO − 3), as well as non-negligible contributions from molecular orbitals of even lower energy (*e.g.*, ϕ_{36}). These orbitals were not included in the active space of the MC-SCF approach. The success of the CIS approach in the calculation of $^1(n_- \rightarrow \pi^*)$ excitations in formaldehyde, acetaldehyde, acetone, formamide, and benzaldehyde is well-documented.[27−31] We are therefore inclined to trust the CIS treatment of the S_1* state of diazirine and adamantyldiazirine. Nevertheless, we concede that the MC-SCF approach possesses certain advantages in the calculation of higher excited states. We also note that our calculations involved discrete geometry optimizations, while Yamamoto *et al*. were able to explore significant regions of the relevant potential energy surfaces.[4] More calculations will probably be required to resolve the apparent discrepancies.

The fact that we did not observe a solvent dependence on the fluorescence lifetime of adamantyldiazirine lends further support to the hypothesis that the primary nonradiative decay pathways in the excited state are *intra*molecular processes such as carbene and/or diazo formation, rather than *inter*molecular processes such as solvent insertion. Such *inter*molecular processes would be expected to exhibit some solvent dependence. While some of the ultimate products of the photolysis of adamantyldiazirine arise from intermolecular chemistry, our data suggest that these are generated from one or more intermediates generated subsequent to depopulation of the diazirine excited state, such as adamantylidene or 2-diazoadamantane. In this we agree with the conclusion of Bonneau and Liu.[16]

Our analysis of the absorption and fluorescence emission spectra in a variety of solvents has demonstrated that adamantyldiazirine possesses a larger dipole moment in S_1* than in S_0, a conclusion that is confirmed by our semiempirical and *ab initio* calculations. We were also able to assign some of the vibrations of adamantyldiazirine.

(51) Michl, J.; Bonacic-Koutecky, V. *Electronic Aspects of Organic Photochemistry*; John Wiley & Sons, Inc.: New York, 1990.
(52) Lathan, W. A.; Radom, L.; Hariharan, P. C.; Hehre, W. J.; Pople, J. A. *Top. Current Chem.* **1973**, *40*, 1−45.

While semiempirical methods and RHF/6-31G* calculations appear to be adequate for the determination of diazirine geometries, we found that vibrational analyses at the MP2(fc)/6-31G* level or higher were required to predict accurately the absolute frequencies of vibrational modes involving the diazirine ring moiety. While electron correlation was required to obtain the absolute frequencies of these modes, the semiempirical, density functional, and Hartree−Fock methods appeared to be adequate to assign the normal modes and evaluate the general nature of the molecular vibrations. The less rigorous calculations also seemed to be capable of calculating the absolute frequencies of modes that did not significantly involve the diazirine ring.

Our data suggest that the N═N stretch experiences a significant reduction in force constant and frequency of vibration upon photoexcitation. In this we concur with earlier investigations of difluorodiazirine by Lombardi *et al.*[40] On the other hand, the vibrational modes localized in the adamantyl cage are relatively unaffected by the excitation. Further investigations of the vibrational spectroscopy and mode-specific behavior of the S_1* state of adamantyldiazirine are in progress.

Acknowledgment. We acknowledge Coherent, Inc., for the loan of some of the equipment used in these experiments. We acknowledge the National Science Foundation for support of portions of the instrumentation used in this work under grants CHE-9528307, CHE-9108384, and CHE-8814950. We also acknowledge the Ohio State University for partial support of this work through the Seed Grant Program and the Centre for Materials Research. J.S.B. is grateful for the invitational orders issued to perform the experiments conducted at Wright-Patterson Air Force Base and acknowledges financial support from a Department of Education National Needs Fellowship. J.P.T. gratefully acknowledges the support of an N.I.H. postdoctoral fellowship. We are grateful to T. Barckholtz for attempting the MP2 vibrational analysis for adamantyldiazirine.

Supporting Information Available: Tables of calculated vibrational frequencies for the ground electronic state of adamantyldiazirine, calculated energies, geometries, and vibrational frequencies for relevant electronic states of adamantyldiazirine, and CIS vertical excited singlet state energies for diazirine at the MP2(fc)/6-31G* optimized geometry (16 pages). See any current masthead page for ordering and Internet access instructions.

JA964022Q